

Self-assembled monolayers of polyoxovanadates with phthalocyaninato lanthanide moieties on gold surfaces

Ricarda Pütt,^a Xinkai Qiu,^b Piotr Kozłowski,^c Hans Gildenast,^a Oliver Linnenberg,^a
Stefan Zahn,^e Ryan C. Chiechi,^{b,*} and Kirill Yu. Monakhov^{d,*}

^a Institut für Anorganische Chemie, RWTH Aachen University, Landoltweg 1, 52074 Aachen, Germany

^b Stratingh Institute for Chemistry & Zernike Institute for Advanced Materials, University of Groningen, Nijenborgh 4, Groningen 9747 AG, Netherlands

^c Faculty of Physics, Adam Mickiewicz University in Poznań, ul. Uniwersytetu Poznańskiego 2, 61-614 Poznań, Poland

^d Leibniz Institute of Surface Engineering (IOM), Permoserstraße 15, 04318 Leipzig, Germany

* Correspondence and requests for materials should be addressed to
K.Y.M. (kirill.monakhov@iom-leipzig.de) or R.C.C. (r.c.chiechi@rug.nl)

Table of contents

1. General analytical methods and chemicals
2. Synthetic procedure
3. Infrared spectra
4. UV-Vis spectra
5. Electrospray ionisation mass spectrometry data of **mono**⁴⁻ and **bis**³⁻
6. Single-crystal X-ray diffraction data of **mono**⁴⁻ and **bis**³⁻
7. Bond valence sum calculations
8. Thermogravimetric data of **mono**⁴⁻ and **bis**³⁻
9. Magnetochemical analysis of **mono**⁴⁻ and **bis**³⁻
10. Computational details
11. EGaln measurement
12. Atomic force microscopy measurements
13. Ellipsometry

1. General analytical methods and chemicals

All starting materials were commercial and used as received. All solvents were dried over CaH_2 and distilled before use.

Elemental analysis (CHN) of compounds was carried out using a Vario EL elemental analyzer.

IR spectra were recorded on a Nicolet Avatar 360 FT-IR-spectrometer by using KBr pellets ($m_{\text{KBr}} \approx 250$ mg) in the 4000–400 cm^{-1} range.

UV-Vis spectra were recorded on a Shimadzu UV-2600 spectrophotometer. The samples were dissolved in dry acetonitrile and measured in quartz cuvettes ($d = 1$ cm).

The ESI-MS spectra were recorded in the positive and negative ion modes using a 4000 QTRAP mass spectrometer system.

Thermogravimetric analysis was performed with a Mettler-Toledo TGA / SDTA 851e under N_2 atmosphere and air with a heating rate of 10 K min^{-1} .

2. Synthetic procedure

$(n\text{Bu}_4\text{N})_4[\text{HV}_{12}\text{O}_{32}(\text{Cl})]$ was synthesised according to the literature¹ and $\text{YbC}_{34}\text{H}_{19}\text{O}_2\text{N}_8 \cdot 2\text{MeOH}$ ($\text{C}_{32}\text{H}_{16}\text{N}_8 = \text{Pc}$) was synthesised similar to the protocol reported in the literature.²

Ytterbium(III)acetate hydrate (2 mmol, calculated on water-free basis) was grinding in a mortar and dried for 2h under vacuum at 100 °C. After cooling down to room temperature phthalonitrile (1.55 g, 12 mmol) was added and dried under vacuum at room temperature. Next, dry *n*-Hexanol (15 mL) and dry 1,8-Diazabicyclo[5.4.0]undec-7-en (0.9 mL, 6 mmol) were successively added under N_2 . The suspension was heated up to 160°C, whereby the suspension gradually clears up. After a few minutes the colour of solution changed to light green and then to dark green. The reaction was stopped after 30 minutes, the heating plate was removed and the solution was cooled down to room temperature under ambient conditions. The resulting viscous solution was precipitated into 200 mL of hexane, affording a nearly black / dark-blue solid. The solid was purified by column chromatography. Using CH_2Cl_2 and MeOH in a 99:1 ratio yields the side product YbPc_2 (dark green). Using CH_2Cl_2 and MeOH in a 95:5 ratio leads to the target product $\text{YbPcOAc} \cdot 2\text{MeOH}$ (dark blue).

Yield: 690 mg (43%).

Elemental analysis (%) calcd. for $\text{C}_{34}\text{H}_{19}\text{N}_8\text{O}_2\text{Yb} \cdot 2\text{MeOH}$ ($M = 808.70 \text{ g mol}^{-1}$): C 53.47, H 3.37, N 13.86; Found: C 53.35, H 3.35, N 13.72.

FT-IR (KBr, $\tilde{\nu}_{\text{max}}/\text{cm}^{-1}$): 3432 (m), 3086 (w), 2924(w), 2854 (w), 2231 (w), 1607 (w), 1570 (w), 1525 (vs), 1472 (m), 1455 (m), 1404 (m), 1361 (s), 1324 (s), 1161 (w), 1116 (m), 1081 (w), 1062 (m), 1040 (w), 1019 (w), 965 (w), 886 (w), 839 (w), 768 (s), 730 (vs), 639 (w), 558 (w), 526 (m), 503 (w), 435 (w).

¹ K. Okaya, T. Kobayashi, Y. Koyama, Y. Hayashi and K. Isobe, *Eur. J. Inorg. Chem.*, 2009, 5156.

² M. Bouvet, P. Bassoul and J. Simon, *Molecular Crystals and Liquid Crystals Science and Technology. Section A. Molecular Crystals and Liquid Crystals*, 1994, **252**, 31.

$(n\text{Bu}_4\text{N})_4[\text{V}_{12}\text{O}_{32}(\text{Cl})]\text{YbC}_{32}\text{H}_{16}\text{N}_8$ (mono⁴⁻)

106.8 mg (0.05 mmol, 1 eq.) of $(n\text{Bu}_4\text{N})_4[\text{HV}_{12}\text{O}_{32}(\text{Cl})]$ and 37.2 mg (0.05 mmol, 1 eq.) of $\text{YbPcOAc}\cdot 2\text{MeOH}$ were dissolved in 5 mL of MeCN using an ultrasonic bath. The solution was allowed to stand for 5 days at room temperature without stirring. The solution was filtered off and the filtrate was dropped into 100 mL of Et_2O . The resulting precipitate was centrifuged 10 min with 9000 rpm and washed two times with 40 mL of Et_2O . The obtained green-blue solid was dried under vacuum.

Yield: 113 mg (80%). **Elemental analysis** (%) calcd. for $(\text{C}_{96}\text{H}_{160}\text{ClN}_{12}\text{O}_{32}\text{V}_{12}\text{Yb})\cdot\text{Et}_2\text{O}$ ($M = 2814.36 \text{ g mol}^{-1}$): C 41.58, H 5.93, N 5.84. Found: C, 41.45, H 5.98, N 5.43. **FT-IR** (KBr, $\tilde{\nu}_{\text{max}}/\text{cm}^{-1}$): 3047 (w), 2960 (m), 2933 (m), 2872 (m), 2534 (w), 1634 (w), 1608 (w), 1586 (w), 1564 (w), 1483 (s), 1458 (m), 1407 (w), 1380 (w), 1329 (s), 1282 (m), 1159 (w), 1112 (s), 1078 (m), 1061 (s), 994 (vs), 886 (m), 827 (m), 767 (m), 743 (s), 733 (vs), 681 (s), 630 (m). **UV-Vis** (MeCN, λ/nm): 222, 240, 337, 608, 644, 674. **ESI-MS** (MeCN, m/z): $[\text{M}+6\text{Bu}_4\text{N}+\text{H}]^{2+}$ 1649.47 (calcd.), 1649.46 (exptl.); $[\text{M}+5\text{Bu}_4\text{N}+\text{H}]^+$ 3056.65 (calcd.), 3056.63 (exptl.); $[\text{M}+2\text{Bu}_4\text{N}+\text{H}]^{2-}$ 1164.90 (calcd.), 1164.90 (exptl.); $[\text{M}+\text{Bu}_4\text{N}+\text{H}]^-$ 2329.80 (calcd.), 2329.81 (exptl.) where $M = \text{V}_{12}\text{O}_{32}\text{ClYbC}_{32}\text{H}_{16}\text{N}_8$.

$(n\text{Bu}_4\text{N})_3[\text{V}_{12}\text{O}_{32}(\text{Cl})](\text{YbC}_{32}\text{H}_{16}\text{N}_8)_2$ (bis³⁻)

75 mg (0.035 mmol, 1 eq.) of $(n\text{Bu}_4\text{N})_4[\text{HV}_{12}\text{O}_{32}(\text{Cl})]$ and 62.7 mg (0.078 mmol, 2.2 eq.) of $\text{YbPcOAc}\cdot 2\text{MeOH}$ were dissolved in 5 mL of MeCN using an ultrasonic bath. The solution was allowed to stand for 2 days without stirring at 70°C. After cooling down to room temperature, the solution was filtered off and the filtrate was dropped into 100 mL of Et_2O . The resulting precipitate was centrifuged and washed two times with 40 mL of Et_2O . The obtained blue solid was dried under vacuum.

Yield: 111 mg (91%). **Elemental analysis** (%) calcd. for $(\text{C}_{112}\text{H}_{140}\text{ClN}_{19}\text{O}_{32}\text{V}_{12}\text{Yb}_2)\cdot 4 \text{Et}_2\text{O}$ ($M = 3552.46 \text{ g mol}^{-1}$): C 43.26, H 5.11, N 7.49. Found: C 43.10, H 5.13, N 7.29. **FT-IR** (KBr, $\tilde{\nu}_{\text{max}}/\text{cm}^{-1}$): 3047 (w), 2960 (m), 2931 (m), 2872 (m), 2534 (w), 1633 (w), 1607 (w), 1586 (w), 1563 (w), 1484 (s), 1457 (m), 1407 (w), 1379 (w), 1329 (s), 1281 (m), 1159 (w), 1112 (s), 1078 (m), 1061 (s), 995 (vs), 886 (m), 810 (m), 770 (m), 743 (s), 732 (vs), 676 (m), 629 (m), 614 (m). **UV-VIS** (MeCN, λ/nm): 222, 240, 336, 608, 642, 671. **ESI-MS** (MeCN, m/z): $[\text{M}+5\text{Bu}_4\text{N}]^+$ 3741.73 (calcd.), 3741.70 (exptl.); $[\text{M}+6\text{Bu}_4\text{N}]^{2+}$ 1992.01 (calcd.), 1992.00 (exptl.); $[\text{M}+2\text{Bu}_4\text{N}]^{2-}$ 1507.44 (calcd.), 1507.43 (exptl.); $[\text{M}+\text{Bu}_4\text{N}]^{2-}$ 1386.30 (calcd.), 1386.31 (exptl.) where $M = \text{V}_{12}\text{O}_{32}\text{ClYb}_2\text{C}_{64}\text{H}_{32}\text{N}_{16}$.

3. Infrared spectra

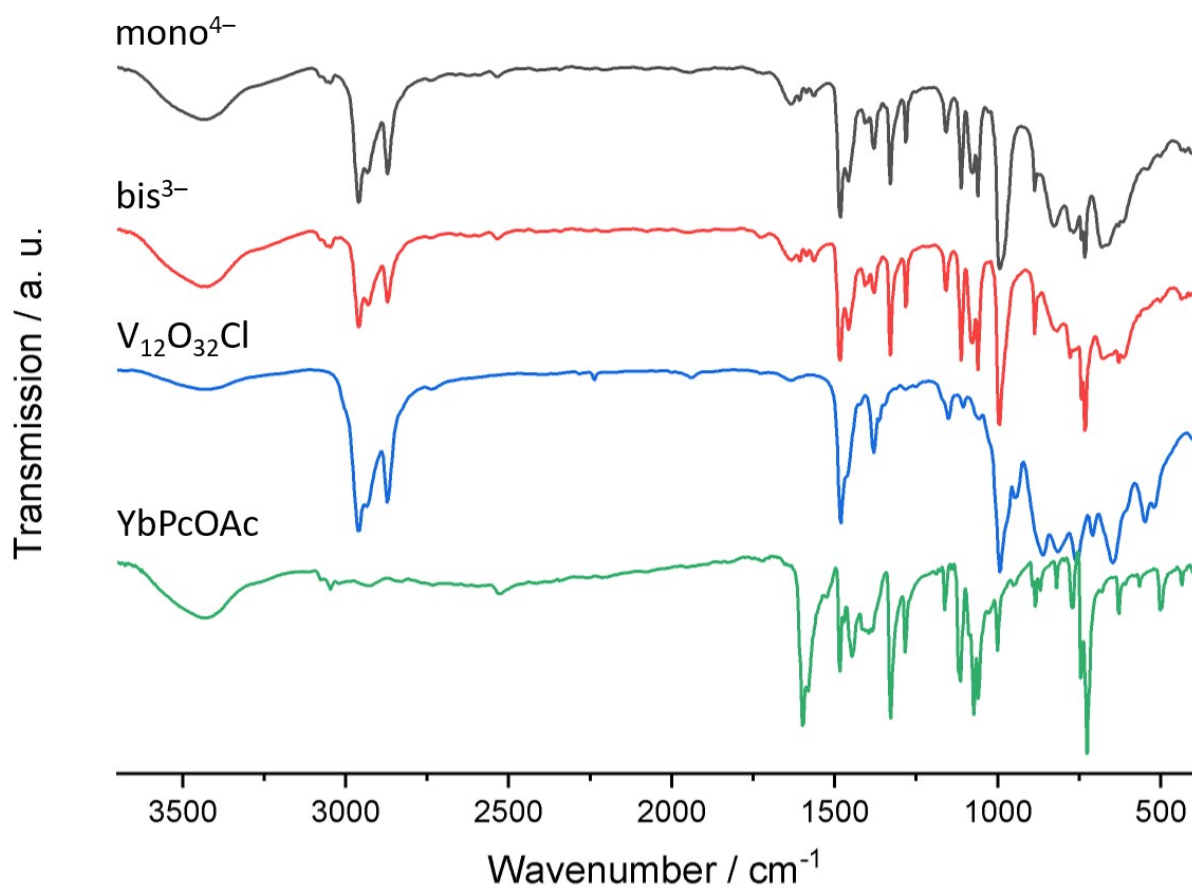


Figure S1. A comparison of IR spectra of **mono⁴⁻**, **bis³⁻**, (*n*Bu₄N)₄[HV₁₂O₃₂(Cl)] (abbreviated as V₁₂O₃₂Cl) and YbPcOAc·2MeOH (abbreviated as YbPcOAc).

4. UV-Vis spectra

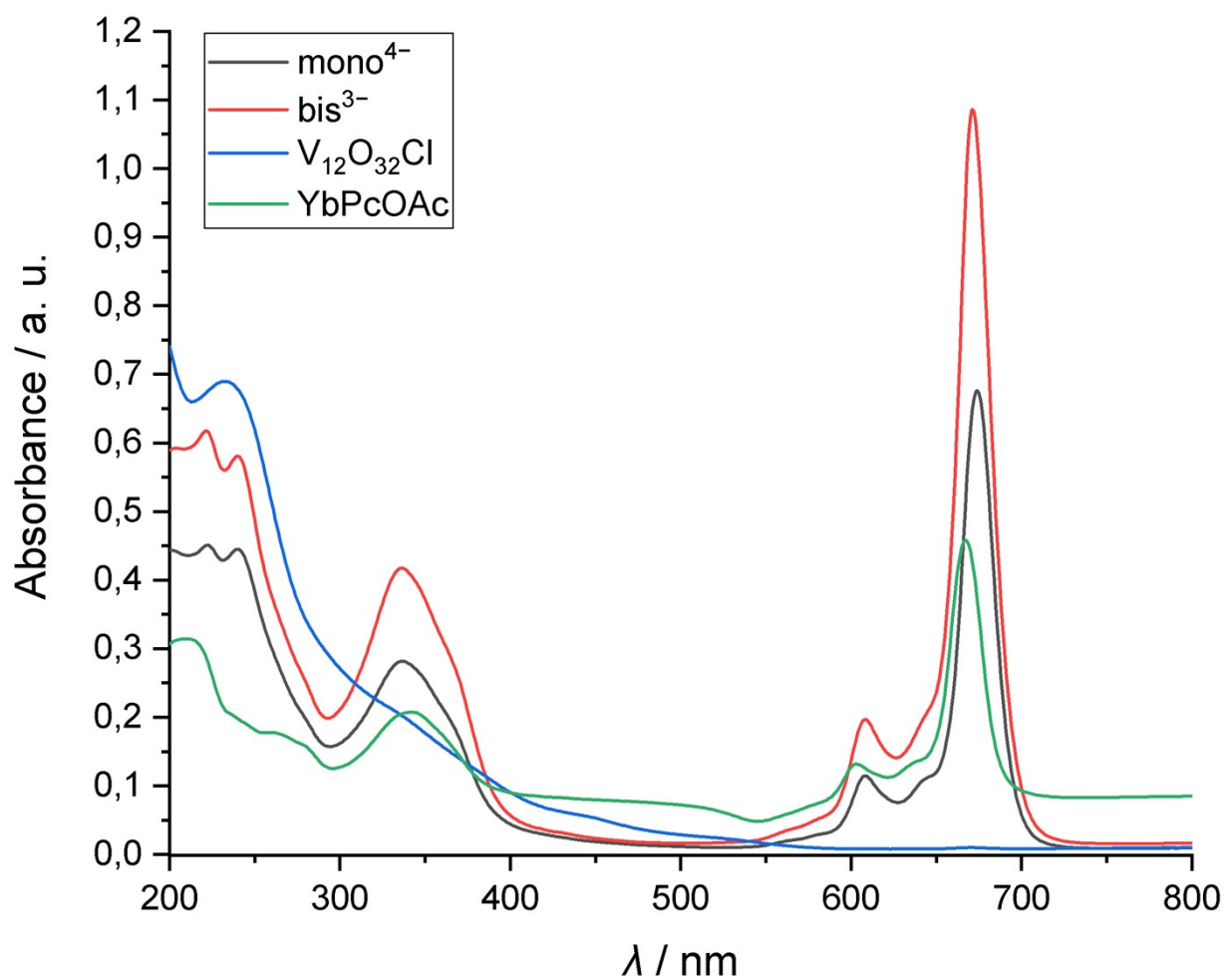


Figure S2. A comparison of UV-VIS spectra of mono^{4-} ($c = 4 \times 10^{-6}$), bis^{3-} ($c = 4 \times 10^{-6}$), $(n\text{Bu}_4\text{N})_4[\text{HV}_{12}\text{O}_{32}(\text{Cl})]$ (abbreviated as $\text{V}_{12}\text{O}_{32}\text{Cl}$; $c = 1.2 \times 10^{-5}$) and $\text{YbPcOAc} \cdot 2\text{MeOH}$ (abbreviated as YbPcOAc ; $c = 2 \times 10^{-5}$). All measurements were performed in MeCN.

5. Electrospray ionisation mass spectrometry data of mono⁴⁻ and bis³⁻

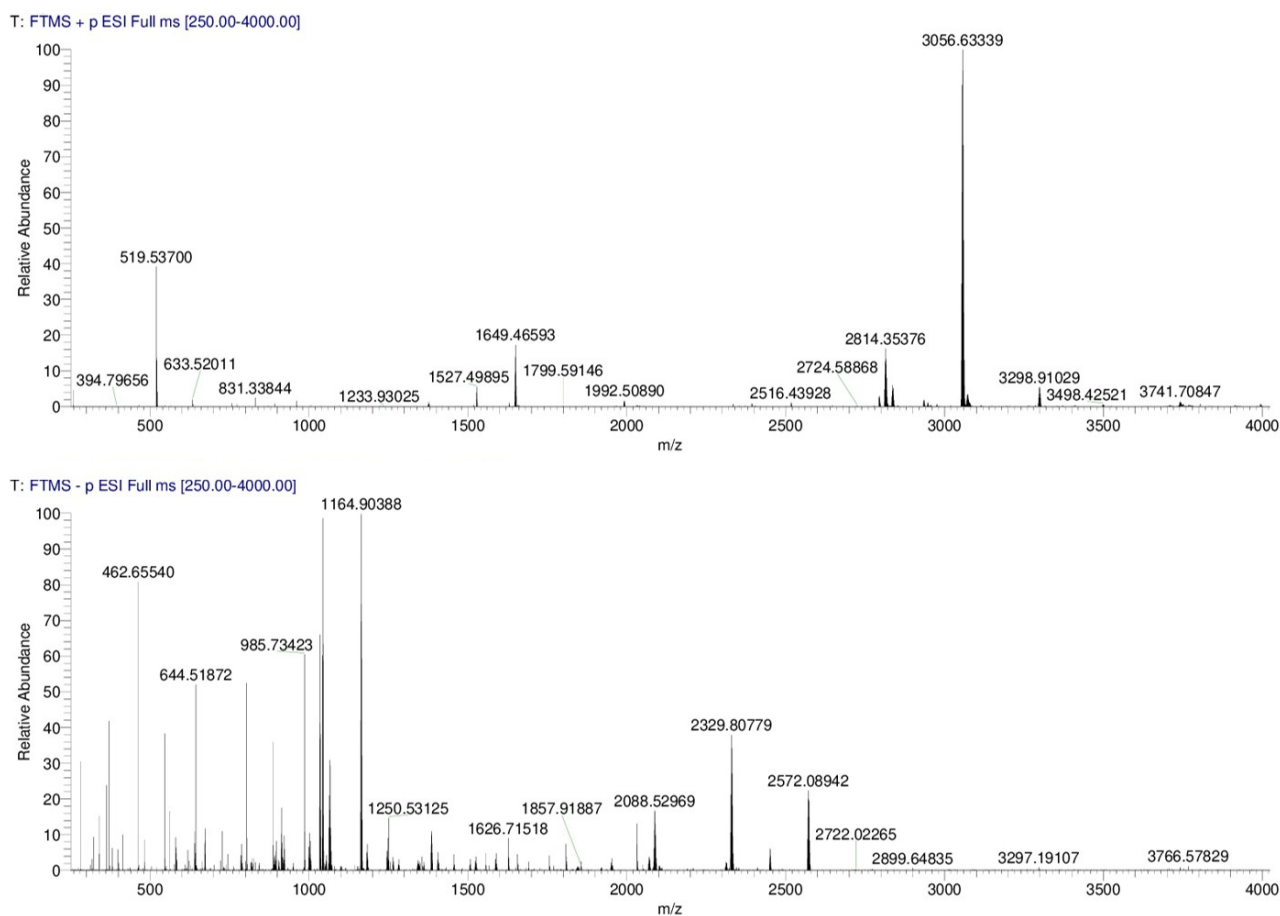


Figure S3. ESI-MS spectra of **mono⁴⁻** (in MeCN) obtained in the positive (top) and negative (bottom) ion modes.

Table S1. Experimental and calculated *m/z* values for different fragments of **mono⁴⁻**.

Fragment ion	<i>m/z</i> exptl.	<i>m/z</i> calcd.
$[(\text{Bu}_4\text{N})_5[\text{HV}_{12}\text{O}_{32}\text{Cl}]\text{Yb}(\text{Pc})]^+$	3056.63	3056.65
$[(\text{Bu}_4\text{N})_4[\text{HV}_{12}\text{O}_{32}\text{Cl}]\text{Yb}(\text{Pc})]^+$	2814.35	2814.37
$[(\text{Bu}_4\text{N})_6[\text{HV}_{12}\text{O}_{32}\text{Cl}]\text{Yb}(\text{Pc})]^{2+}$	1649.46	1649.47
$[(\text{Bu}_4\text{N})_3[\text{HV}_{12}\text{O}_{32}\text{Cl}]\text{Yb}(\text{Pc})]^-$	2572.09	2572.08
$[(\text{Bu}_4\text{N})_2[\text{HV}_{12}\text{O}_{32}\text{Cl}]\text{Yb}(\text{Pc})]^-$	2329.81	2329.80
$[(\text{Bu}_4\text{N})_2[\text{HV}_{12}\text{O}_{32}\text{Cl}]\text{Yb}(\text{Pc})]^{2-}$	1164.90	1164.90

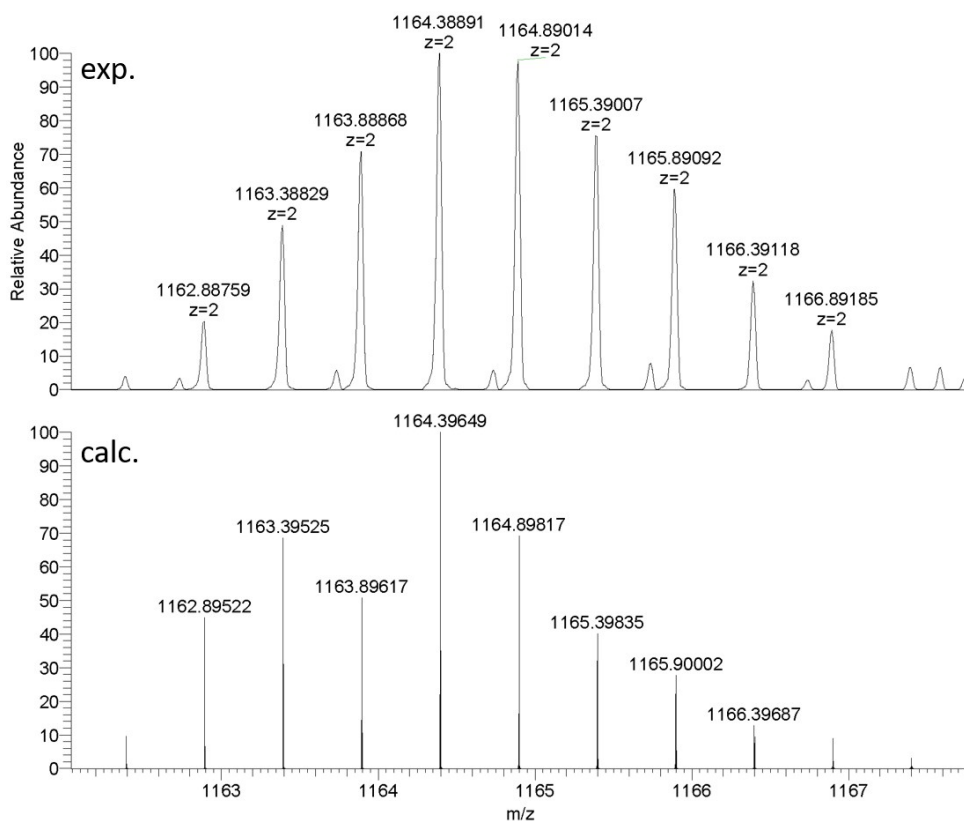


Figure S4. Experimental and calculated isotopic patterns of $[(\text{Bu}_4\text{N})_2[\text{V}_{12}\text{O}_{32}\text{Cl}]\text{Yb}(\text{Pc})]^{2-}$ fragment in mono^{4-} .

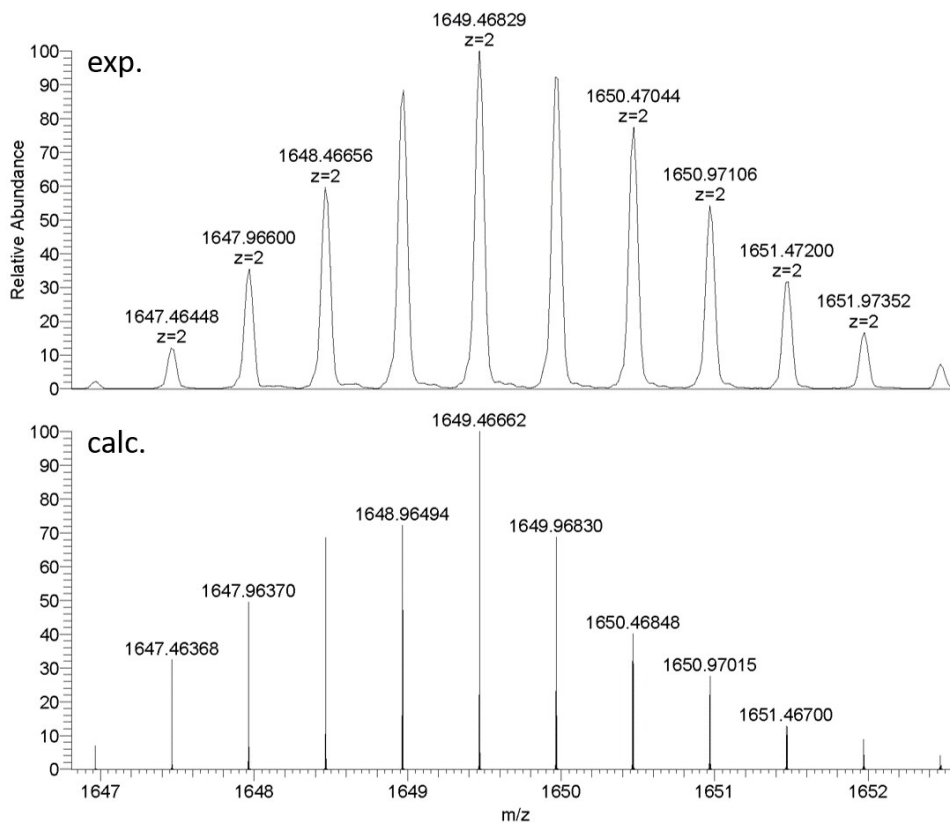


Figure S5. Experimental and calculated isotopic patterns of $[(\text{Bu}_4\text{N})_6[\text{HV}_{12}\text{O}_{32}\text{Cl}]\text{Yb}(\text{Pc})]^{2+}$ fragment in mono^{4-} .

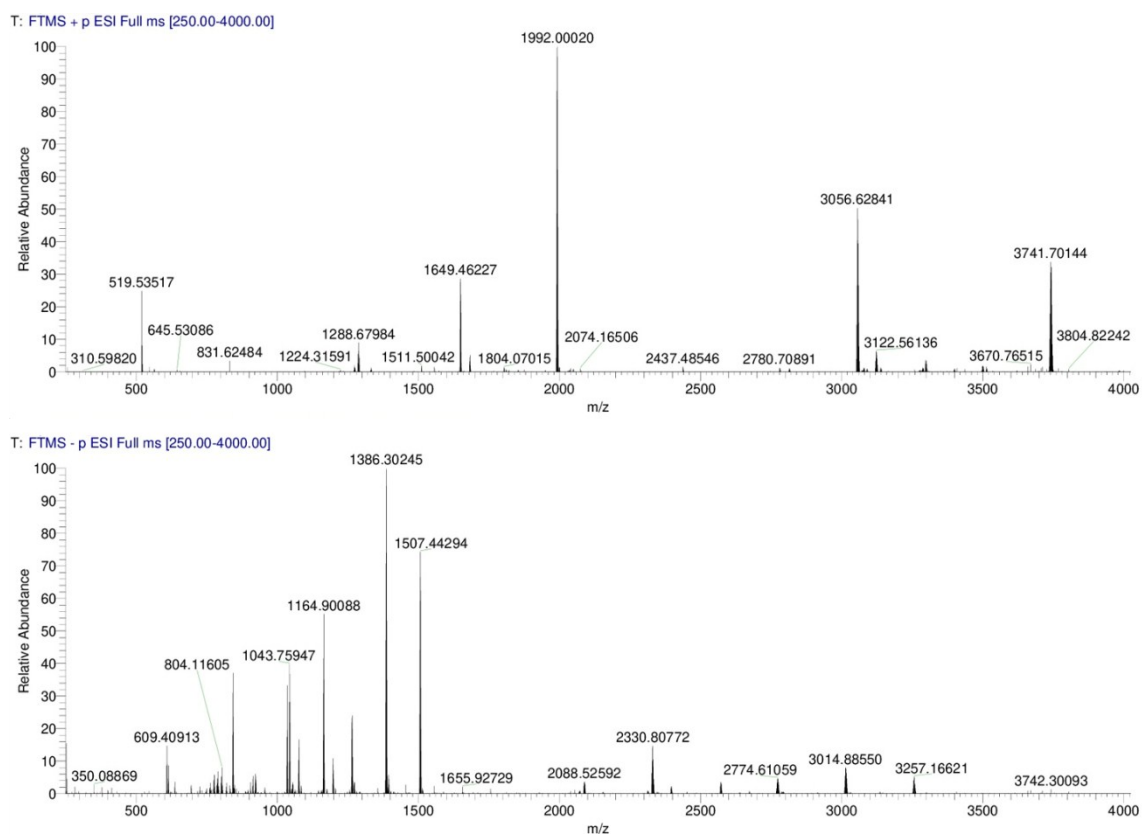


Figure S6. ESI-MS spectra of **bis³⁻** (MeCN) obtained in the positive (top) and negative (bottom) ion modes.

Table S2. Experimental and calculated *m/z* values for different fragments of **bis³⁻**.

Fragment ion	<i>m/z</i> exptl.	<i>m/z</i> calcd.
$[(\text{Bu}_4\text{N})_5[\text{V}_{12}\text{O}_{32}\text{Cl}](\text{YbPc})_2]^+$	3741.70	3741.73
$[(\text{Bu}_4\text{N})_5[\text{HV}_{12}\text{O}_{32}\text{Cl}](\text{YbPc})]^+$	3056.63	3056.65
$[(\text{Bu}_4\text{N})_6[\text{V}_{12}\text{O}_{32}\text{Cl}](\text{YbPc})_2]^{2+}$	1992.00	1992.01
$[(\text{Bu}_4\text{N})_6[\text{HV}_{12}\text{O}_{32}\text{Cl}](\text{YbPc})]^{2+}$	1649.46	1649.47
$[(\text{Bu}_4\text{N})_3[\text{V}_{12}\text{O}_{32}\text{Cl}](\text{YbPc})_2]^-$	3257.17	3257.17
$[(\text{Bu}_4\text{N})_2[\text{V}_{12}\text{O}_{32}\text{Cl}](\text{YbPc})_2]^-$	3014.89	3014.88
$[(\text{Bu}_4\text{N})[\text{H}_2\text{V}_{12}\text{O}_{32}\text{Cl}](\text{YbPc})_2]^-$	2774.61	2774.61
$[(\text{Bu}_4\text{N})_3[\text{HV}_{12}\text{O}_{32}\text{Cl}](\text{YbPc})]^-$	2572.10	2572.08
$[(\text{Bu}_4\text{N})_2[\text{H}_2\text{V}_{12}\text{O}_{32}\text{Cl}](\text{YbPc})]^-$	2330.81	2330.80
$[(\text{Bu}_4\text{N})_2[\text{V}_{12}\text{O}_{32}\text{Cl}](\text{YbPc})_2]^{2-}$	1507.43	1507.44
$[(\text{Bu}_4\text{N})[\text{V}_{12}\text{O}_{32}\text{Cl}](\text{YbPc})_2]^{2-}$	1386.30	1386.30
$[(\text{Bu}_4\text{N})_2[\text{HV}_{12}\text{O}_{32}\text{Cl}](\text{YbPc})]^{2-}$	1164.90	1164.90

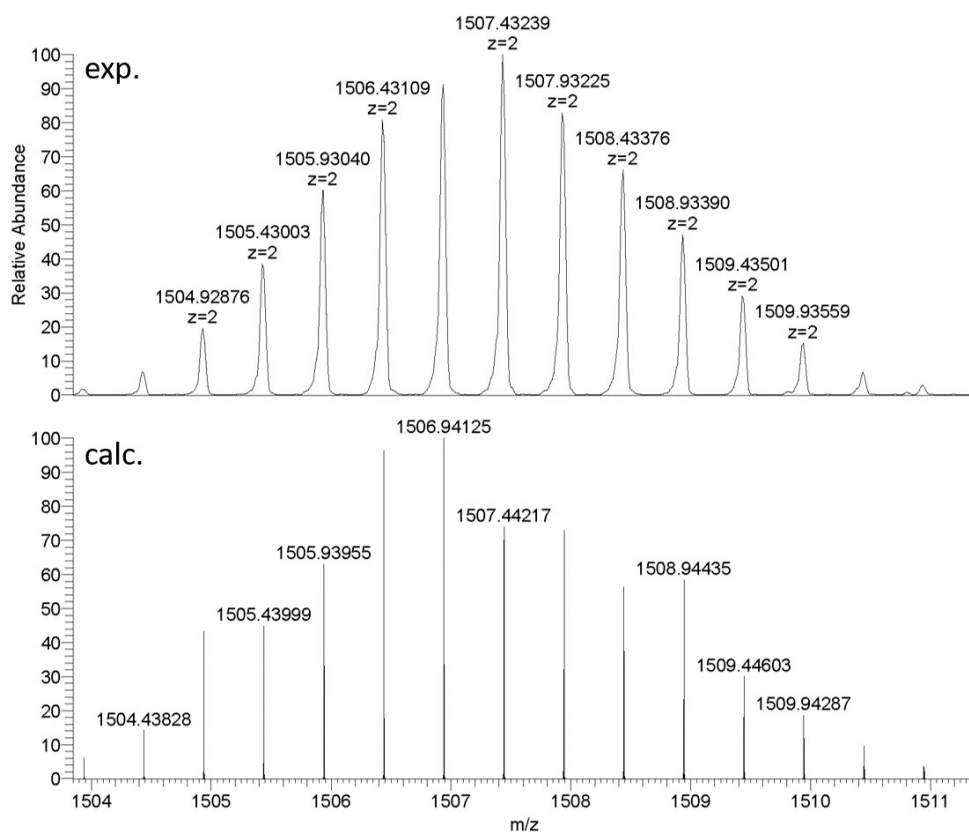


Figure S7. Experimental and calculated isotopic patterns of $[(\text{Bu}_4\text{N})_2[\text{V}_{12}\text{O}_{32}\text{Cl}](\text{YbPc})_2]^{2-}$ fragment in bis^{3-} .

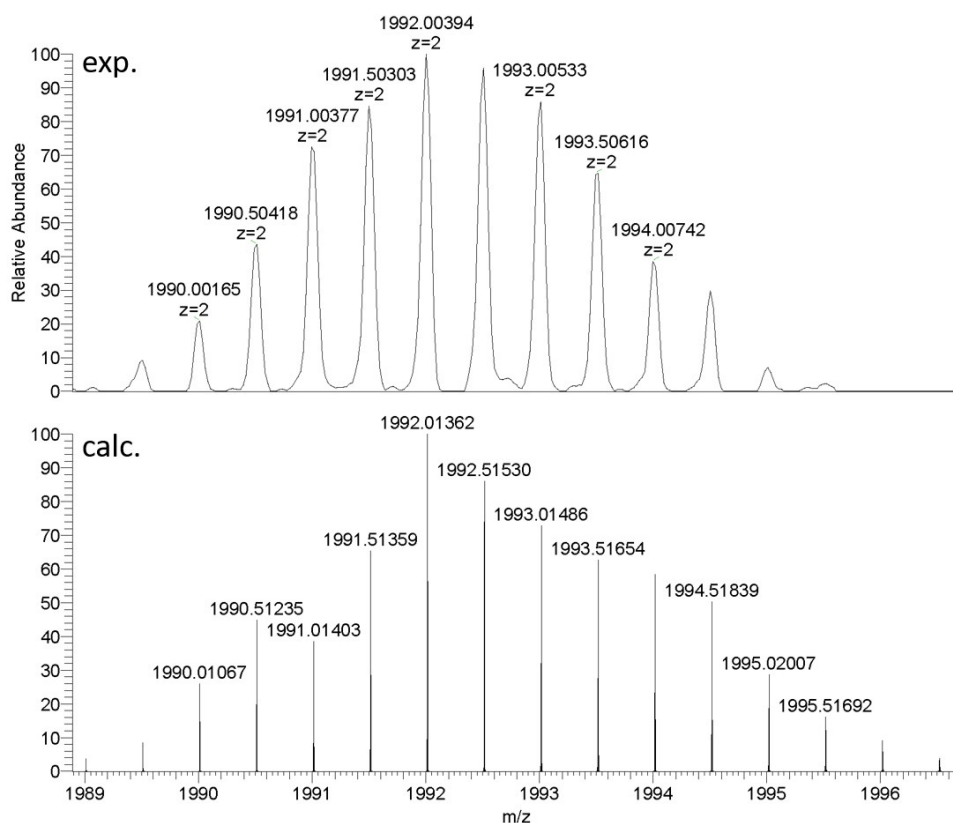


Figure S8. Experimental and calculated isotopic patterns of $[(\text{Bu}_4\text{N})_6[\text{V}_{12}\text{O}_{32}\text{Cl}](\text{YbPc})_2]^{2+}$ fragment in bis^{3-} .

6. Single-crystal X-ray diffraction data of mono⁴⁻ and bis³⁻

Table S3. Crystal data and structure refinement details for compounds.

	mono ⁴⁻	bis ³⁻
CCDC	1950768	1950769
Empirical formula	C ₂₃₀ H ₄₀₉ Cl ₂ N ₂₇ O ₇₂ V ₂₄ Yb ₂	C ₁₂₀ H ₁₅₂ ClN ₂₃ O ₃₂ V ₁₂ Yb ₂
Chemical formula	2[(C ₁₆ H ₃₂ N) ₄ (YbC ₃₂ H ₁₆ N ₈ V ₁₂ O ₃₂ Cl)] (CH ₃ CN) ₃ ((CH ₃ CH ₂) ₂ O) ₈	(C ₁₆ H ₃₂ N) ₃ (Yb ₂ C ₆₄ H ₃₂ N ₁₆ V ₁₂ O ₃₂ Cl) (CH ₃ CN) ₄
Formula weight	6343.04	3421.52
Crystal colour	green	blue
Crystal system	orthorhombic	tetragonal
<i>T</i> / K	100(2)	100(2)
Wavelength λ	0.71073 (MoK α)	0.71073 (MoK α)
space group (No.)	<i>Pbca</i> (61)	I-4 (82)
<i>a</i> / Å	30.109(6)	14.840(3)
<i>b</i> / Å	29.594(6)	14.840(3)
<i>c</i> / Å	33.020(7)	35.452(8)
α / °	90	90
β / °	90	90
γ / °	90	90
<i>V</i> / Å ³	29422(10)	7808(4)
<i>Z</i>	4	2
<i>R</i> _{int}	0.1834	0.1157
Absorp. Coeff. μ / mm ⁻¹	1.443	1.951
<i>R</i> [<i>F</i> ² > 2 σ (<i>F</i> ²)]	0.0671	0.0777
<i>wR</i> ₂ (<i>F</i> ²)	0.2284	0.2347
<i>D</i> _{calcd.} / g cm ⁻³	1.432	1.418
GOF	0.744	1.016

Table S4. Selected bond lengths (Å).

Bonds		mono ⁴⁻	Bonds		bis ³⁻
Yb01	O00R	2.306(7)	Yb01	N00M ¹	2.26(4)
Yb01	O013	2.328(7)	Yb01	N00M	2.26(4)
Yb01	O00F	2.334(6)	Yb01	O008 ¹	2.35(2)
Yb01	O011	2.340(6)	Yb01	O008	2.35(2)
Yb01	N00W	2.352(8)	Yb01	O07 ¹	2.35(2)
Yb01	N00Z	2.358(7)	Yb01	O07	2.335(2)
Yb01	N01D	2.353(8)	Yb01	N00E	2.42(3)
Yb01	N01G	2.355(8)	Yb01	N00E	2.42(3)
V00D	O01B	1.987(7)	V004	O009	2.03(2)
V00D	O014	1.925(7)	V004	O00C	1.90(3)
V00D	O012	1.826(7)	V004	O07	1.84(2)
V00D	O019	1.774(7)	V004	O00D	1.80(2)
V00D	O017	1.576(8)	V004	O0B	1.59(2)
V00C	O01B	1.936(8)	V003	O06	1.62(2)
V00C	O012	1.810(7)	V003	O07	1.87(2)
V00C	O00K	1.814(8)	V003	O008	1.86(2)
V00C	O016	1.603(7)	V003	O00C	1.88(2)
V00C	O00Q	1.940(7)	V003	O009	1.93(2)
V00B	O00Y	1.923(7)	V002	O00C	1.979(2)
V00B	O00K	1.815(8)	V002	O008	1.84(2)
V00B	O01E	1.784(6)	V002	O009	1.84(2)
V00B	O00X	1.592(7)	V002	O00D	1.78(2)
V00B	O00Q	1.982(7)	V002	O0A	1.58 (2)
V00A	O013	1.886(6)			
V00A	O011	1.885(7)			
V00A	O014	1.877(7)			
V00A	O018	1.856(6)			
V00A	O0P	1.586(7)			
V009	O015	1.923(7)			
V009	O00H	1.817(6)			
V009	O00O	1.810(7)			
V009	O0I	1.585(7)			
V009	O00V	1.938(7)			
V008	O00R	1.892(6)			
V008	O00F	1.882(7)			
V008	O00Y	1.869(6)			
V008	O01A	1.855(6)			
V008	O0L	1.589(7)			
V007	O015	1.981(6)			
V007	O01A	1.948(7)			
V007	O01E	1.804(6)			
V007	O00H	1.802(7)			
V007	O00U	1.577(8)			
V006	O0N	1.796(7)			
V006	O014	2.010(7)			
V006	O01B	1.882(7)			
V006	O013	1.836(6)			

V006	O010	1.589(7)
V005	O018	1.955(7)
V005	O0J	1.589(7)
V005	O00O	1.803(7)
V005	O019	1.811(7)
V005	O00V	1.975(7)
V004	O011	1.838(6)
V004	O018	1.986(7)
V004	O00T	1.785(7)
V004	O00S	1.591(6)
V004	O00V	1.898(7)
V003	O01A	2.000(6)
V003	O015	1.905(7)
V003	O00R	1.839(6)
V003	O00T	1.790(7)
V003	O0G	1.590(7)
V002	O00Y	1.994(7)
V002	O00Q	1.891(7)
V002	O00F	1.836(6)
V002	O0N	1.789(7)
V002	O0M	1.588(7)

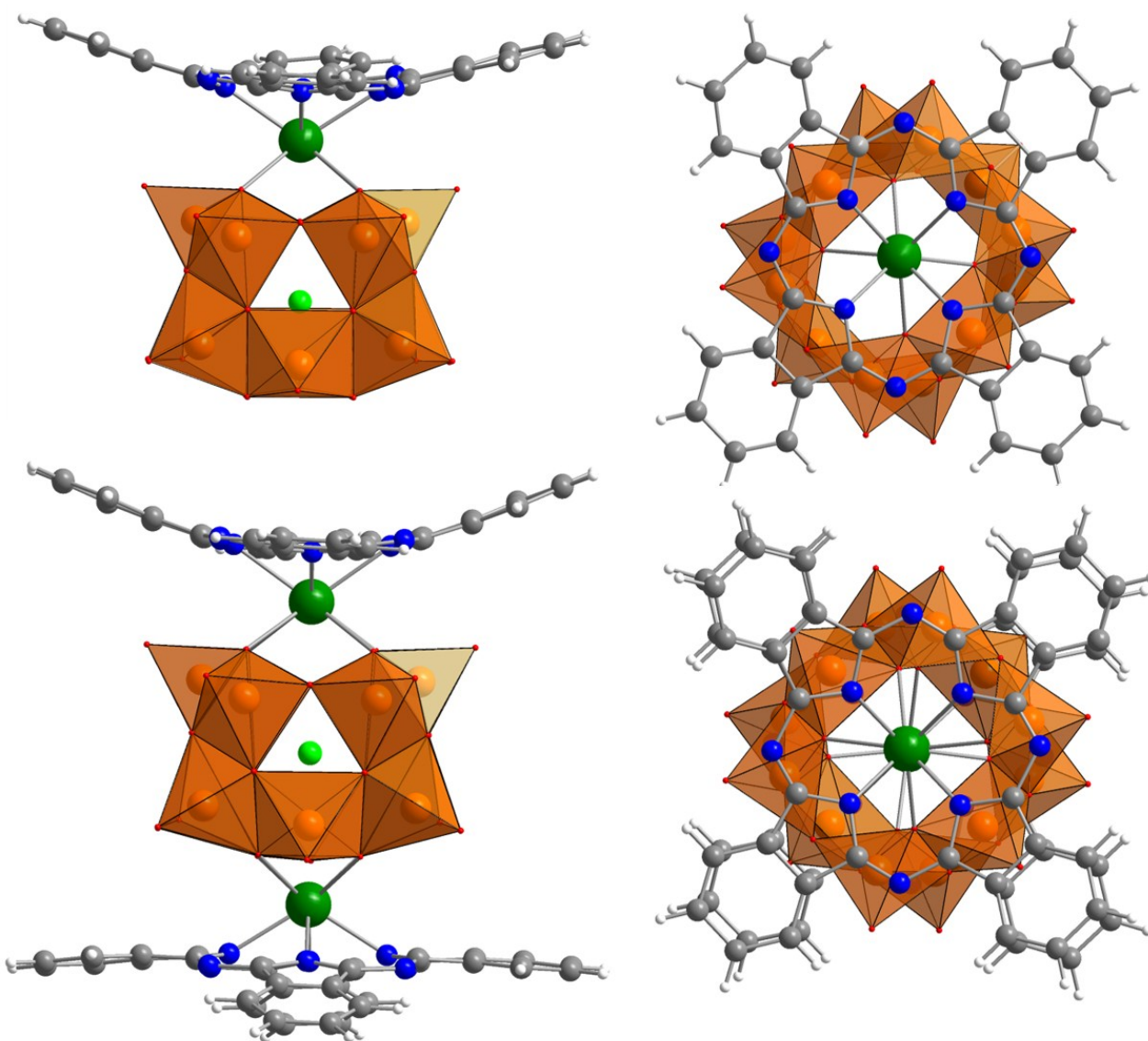


Figure S9. Molecular structures of **mono⁴⁻** (top) and **bis³⁻** (bottom).

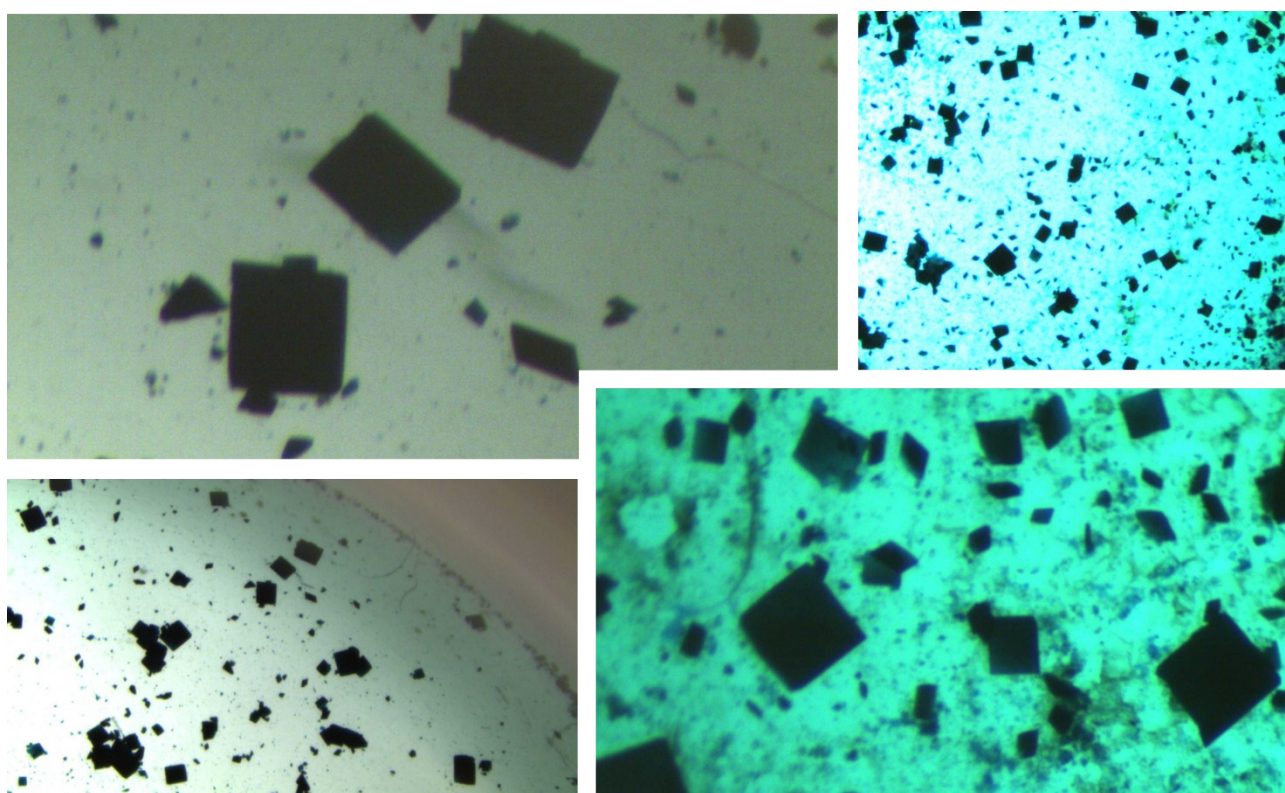
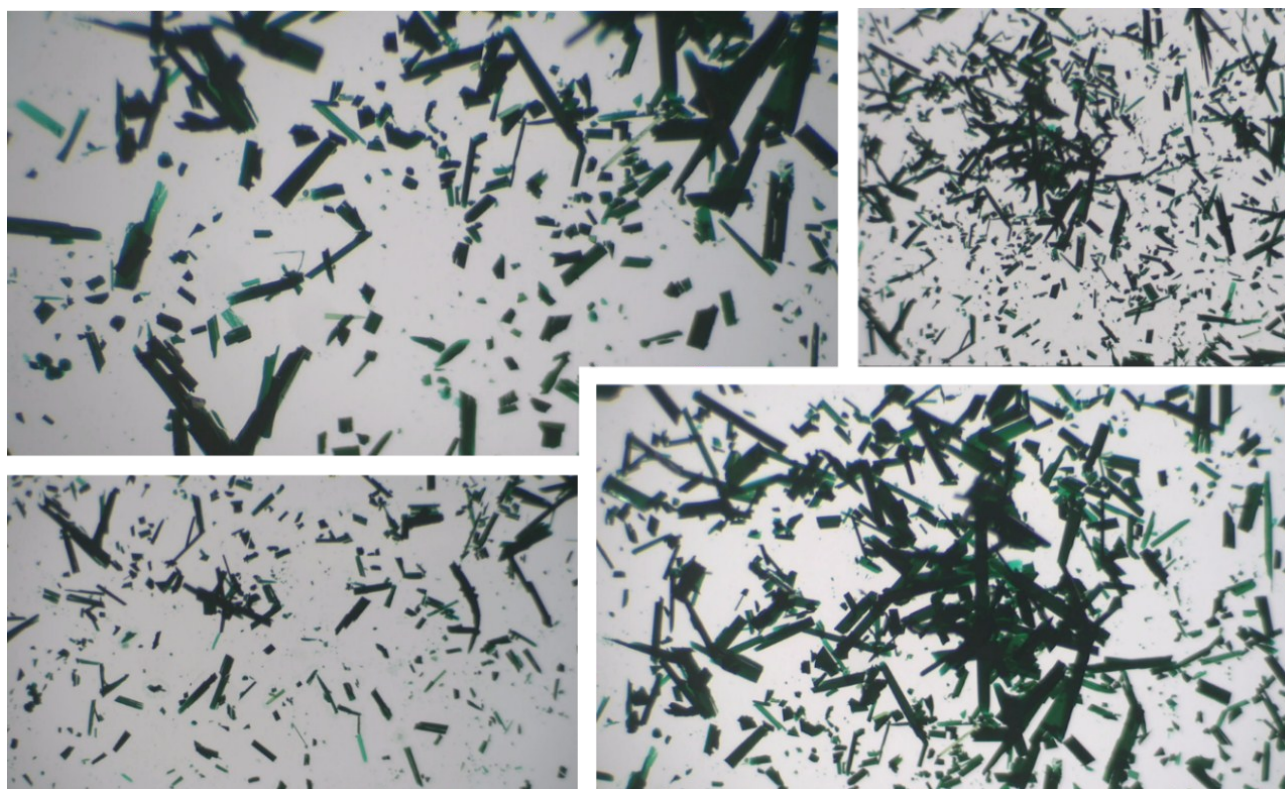


Figure S10. Photographs of characteristic needle-shaped crystals of **mono⁴⁻** (top) and square-shaped crystals of **bis³⁻** (bottom).

7. Bond valence sum calculations

$$BVS = \sum_{n=0}^N \exp \frac{(R_0 - R)}{B}$$

The following parameters for R_0 with $B = 0.37$ were used:^{3,4}

$V^V-(\mu-O)/ V^V-(\mu_3-O)/ V^V-O_{\text{term}}$	$R_0 = 1.803 \text{ \AA}$
$V^{IV}-(\mu-O)/ V^{IV}-(\mu_3-O)$	$R_0 = 1.784 \text{ \AA}$
$V^{IV}-O_{\text{term}}$	$R_0 = 1.735 \text{ \AA}$
$Yb^{II}-O$	$R_0 = 1.989 \text{ \AA}$
$Yb^{II}-N$	$R_0 = 2.092 \text{ \AA}$
$Yb^{III}-O$	$R_0 = 1.954 \text{ \AA}$
$Yb^{III}-N$	$R_0 = 2.064 \text{ \AA}$

Table S5. Acquired BVS data for **mono**⁴⁻ and **bis**³⁻.

Compound	Obtained valence sum (min–max)
mono ⁴⁻ (V^V)	5.06 (4.99–5.13)
mono ⁴⁻ (Yb^{III})	2.81
bis ³⁻ (V^V)	5.04 (4.80–5.26)
bis ³⁻ (Yb^{III})	2.80

³ I. D. Brown, *The Chemical Bond in Inorganic Chemistry: The Bond Valence Model*, Oxford University Press, New York, 2002.

⁴ For bond valence parameters, see www.iucr.org.

8. Thermogravimetric data of mono⁴⁻ and bis³⁻

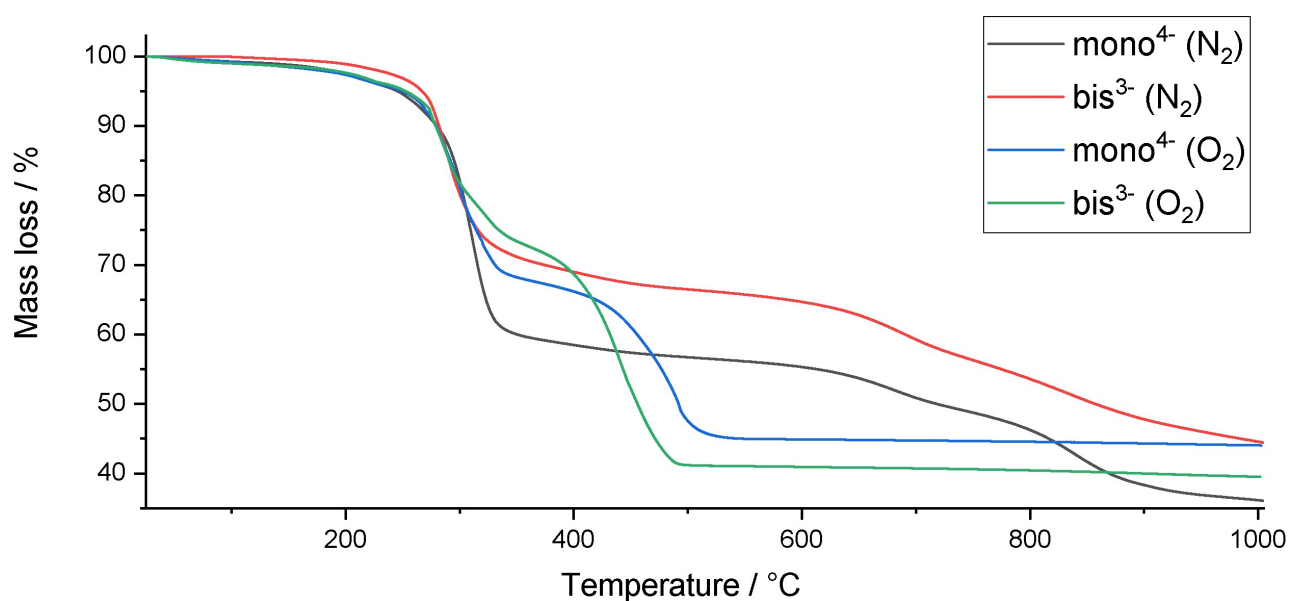


Figure S11. TGA curves of **mono⁴⁻** and **bis³⁻** measured under nitrogen atmosphere and in dry air.

Table S6. Acquired TGA data for **mono⁴⁻** and **bis³⁻**.

Compound	Fragments	$\Delta\omega\%$ (exptl.)	$\Delta\omega\%$ (calcd.)
mono⁴⁻ (N ₂)	-Et ₂ O, -4(Bu ₄ N)	36.75	37.10
mono⁴⁻ (air)	-Et ₂ O, -4(Bu ₄ N), -Pc, -Cl	55.58	56.57
bis³⁻ (N ₂)	-4(Et ₂ O), -3(Bu ₄ N)	28.82	28.54
bis³⁻ (air)	-Et ₂ O, -3(Bu ₄ N), -Pc, -Cl	59.67	58.67

9. Magnetochemical analysis of mono⁴⁻ and bis³⁻

Assuming only the lowest multiplet and C_{2v} symmetry of the molecules a following effective Hamiltonian for **mono⁴⁻** can be proposed:

$$H = H_Z + H_{CF} \quad (1)$$

With the Zeeman part defined as:

$$H_Z = -\mu_B J g B,$$

where \mathbf{J} ($J = 7/2$) is a vector operator standing for a total (orbital and spin) moment, \mathbf{B} is a vector of external magnetic field and \mathbf{g} is a g-factor tensor with non-zero values $g_{xx} = g_x$, $g_{yy} = g_y$ and $g_{zz} = g_z$. The crystal field part H_{CF} should contain up to 9 different Stevens operators.⁵ It is assumed that the z-axis is along the line connecting Yb³⁺ and Cl⁻ centers.

Hamiltonian (1) has together 12 parameters (3 in the Zeeman part and 9 in the crystal field part) that should be determined by fitting the experimental data. This is indeed too many to expect unique solution, especially that we have in disposition only the results for a powder sample. Therefore, the fits were made with smaller number of parameters. It appears that already with three parameters (g_{\perp} , g_{\parallel} and D) one can obtain a good fit for the unique set of optimal parameters. Thus, to obtain the results presented in this study the following simplified Hamiltonian has been used:

$$H = -\mu_B g_{\perp} (J_x B_x + J_y B_y) - \mu_B g_{\parallel} J_z B_z + D J_z^2 \quad (2)$$

With more parameters (we tried up to 6) the fits become a bit better, but there is no unique set of optimal parameters. It seems that despite formally lower symmetry (C_{2v}) **mono⁴⁻** can be simulated with the formula corresponding to higher C_{4v} symmetry. Since measurements were made for a powder sample and the molecule is highly anisotropic the theoretical results have been averaged over possible orientations of the magnetic field with respect to molecular axes. To this end for each value of T (for susceptibility) and B (for magnetisation)

⁵ C. Görrler-Walrand and K. Binnemans, Rationalization of Crystal-Field Parametrization, In *Handbook on the Physics and Chemistry of Rare Earths*, 1996, **23**, 121.

400 orientations of the magnetic field vector uniformly distributed over the hemisphere have been considered. Fits have been performed with the help of evolutionary algorithm.

The same procedure has been applied to **bis**³⁻ resulting in similar conclusions. Here Hamiltonian (1) and (2) must be multiplied by factor 2 to account for two non-interacting Yb³⁺ centers. The results are presented in Figs. 2 and S10, and in Table S7. The fits for **bis**³⁻ are slightly worse than for **mono**⁴⁻. In both cases magnetisation in high field is underestimated by the theory. A point that needs explanation.

Table S7. Optimal parameters of fits.

Compound	g_{\perp}	g_{\parallel}	D / K	goodness of fit in %
mono ⁴⁻	1.16	2.35	170	2.88
bis ³⁻	1.15	1.81	90	4.11

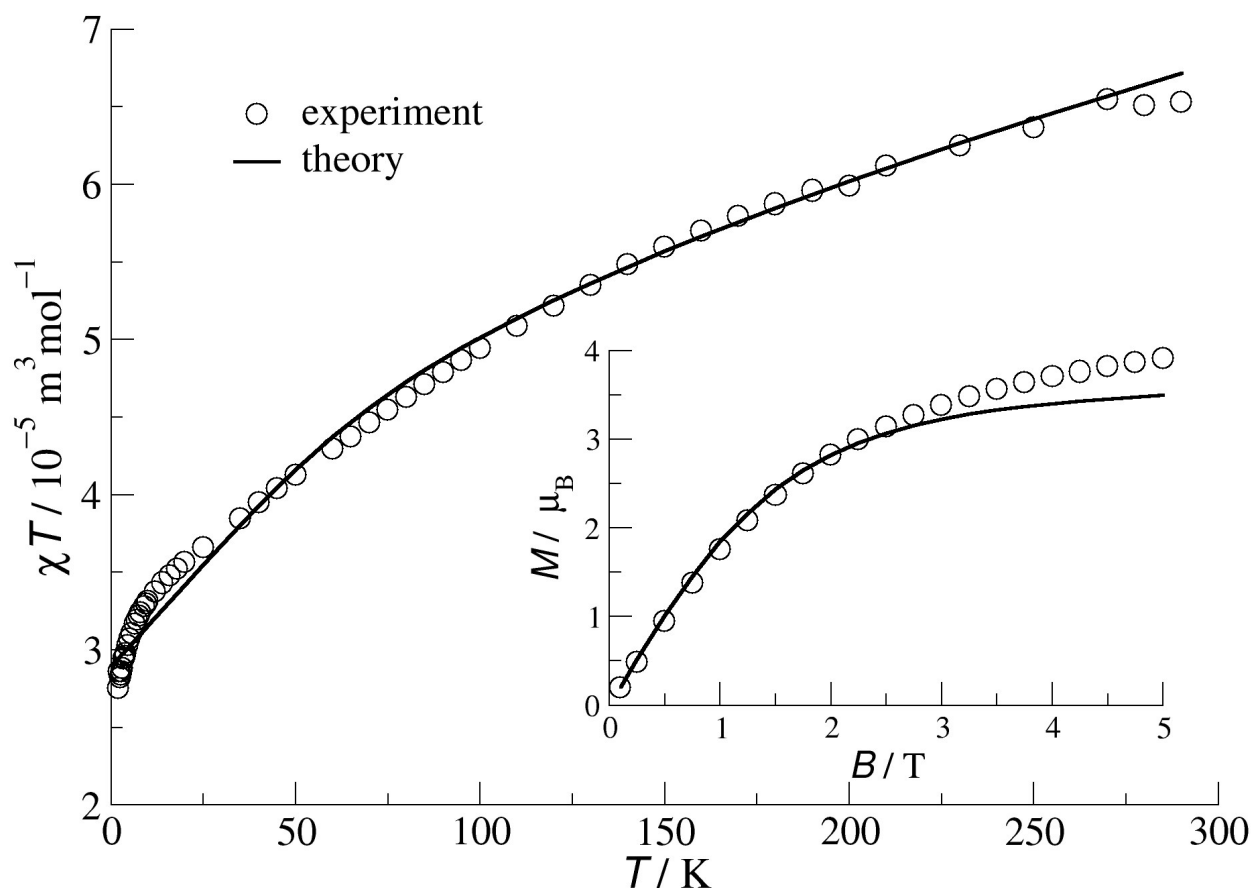


Figure S12. Molar susceptibility ($B = 0.1 \text{ T}$) and magnetisation ($T = 2 \text{ K}$) for polycrystalline powder sample of **bis**³⁻ (circles) with theoretical fits (solid lines).

10. Computational details

All DFT calculations were carried out with the ORCA program package.⁶ Structures were optimised with the B3LYP functional^{7,8,9} where dispersion forces were considered by the 3rd version of Grimme's empirical dispersion correction in combination with Becke-Johnson damping.^{10,11} The Ahlrichs basis set TZVP¹² of triple- ζ quality and polarization functions on all atoms were chosen for N, O, Cl and V, while the smaller double- ζ basis set def2-SV(P)¹³ was employed for C and H. For Yb, the def2-TZVP basis set was chosen including a relativistic pseudopotential.^{13,14} To speed up the calculation, the RIJCOSX approach was employed.^{15,16,17,18} Solvation effects of acetonitrile were considered by the Conductor-like Polarizable Continuum Model (C-PCM).¹⁹

⁶ F. Neese, F. *WIREs Comput. Mol. Sci.*, 2012, **2**, 73.

⁷ A. D. Becke, *Phys. Rev. A*, 1988, **38**, 3098.

⁸ C. Lee, W. Yang and R. G. Parr, *Phys. Rev. B*, 1988, **37**, 785.

⁹ A. D. Becke, *J. Chem. Phys.*, 1993, **98**, 5648.

¹⁰ S. Grimme, J. Antony, S. Ehrlich and H. Krieg, *J. Chem. Phys.*, 2010, **132**, 154104.

¹¹ S. Grimme, S. Ehrlich and L. Goerigk, *J. Comput. Chem.*, 2011, **32**, 1456.

¹² A. Schäfer, C. Huber and R. Ahlrichs, *J. Chem. Phys.*, 1994, **100**, 5829.

¹³ F. Weigend and R. Ahlrichs, *Phys. Chem. Chem. Phys.*, 2005, **7**, 3297.

¹⁴ M. Dolg, H. Stoll and H. Preuss, *J. Chem. Phys.*, 1989, **90**, 1730.

¹⁵ B. I. Dunlap, J. W. D. Connolly and J. R. Sabin, *J. Chem. Phys.*, 1979, **71**, 3396.

¹⁶ E. J. Baerends, D. E. Ellis and P. Ros, *Chem. Phys.*, 1973, **2**, 41.

¹⁷ F. Weigend, *Phys. Chem. Chem. Phys.*, 2006, **8**, 1057.

¹⁸ F. Neese, F. Wennmohs, A. Hansen and U. Becker, *Chem. Phys.*, 2009, **356**, 98.

¹⁹ V. Barone, M. Cossi and J. Tomasi, *J. Comput. Chem.*, 1998, **19**, 404.

11. EGaIn measurement

The electrical measurement with EGaIn was performed under ambient conditions. In the measurement, the sample was grounded and the EGaIn was biased. At least three samples were examined for SAMs of **mono**⁴⁻ and **bis**³⁻. The potential windows included the following: 0 V → 1 V → -1 V → 0 V, steps of 0.05 V. A total of 5 trace/retrace cycles were recorded for each junctions, and shorts occurred during the measurement (short upon contact with a bias of 1 V or during the cycle) were counted for a failure of junction.

12. Atomic Force Microscopy measurements

PeakForce Tapping AFM and PFQNM AFM measurements were performed on a Bruker AFM multimode MMAFM-2 model. Pure SAMs of **mono**⁴⁻ and **bis**³⁻ were characterised by AFM on both morphology and surface adhesion. PeakForce Tapping AFM was performed with a ScanAsyst-Air probe (resonant frequency 70 kHz, spring constant 0.4 N/m, Bruker) to characterise the surface morphology of the samples at a scan rate of 0.7 Hz and 768 samples per line. The data were analysed with Nanoscope Analysis 1.5 provided by Bruker. Measurements of adhesion were performed in the PFQNM mode. The samples were contacted with a silicon nitride tip with a nominal radius of 1 nm (SAA-HPI-SS, Bruker, resonant frequency 55 kHz, spring constant 0.25 N/m). The deflection sensitivity, spring constant of the cantilever and tip radius were calibrated both before and after the measurement. Samples were scanned at 1 μ m and 500 μ m at a rate of 0.7 Hz and 640 samples per line. Adhesion of the samples were measured under a force load of 0.3 nN.

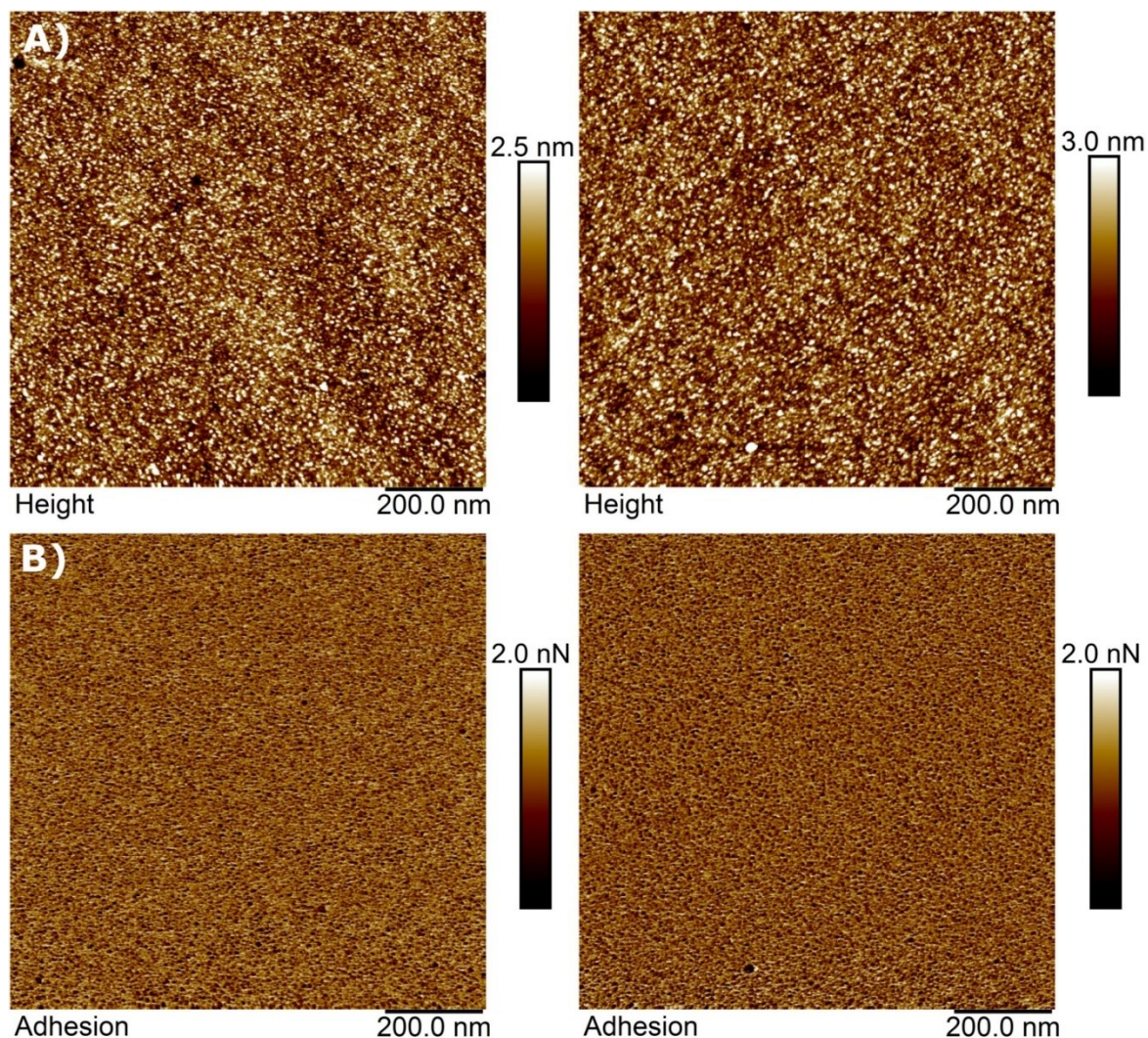


Figure S13. AFM height (a) and adhesion (b) images of SAMs of **mono⁴⁻** (left) and **bis³⁻** (right) on Au^{TS} scanned at 1 μ m. The interaction between the AFM tip and the Au substrate results in stronger adhesion, while the complexes exhibit weaker adhesion to the tip and appear as dark spots in the image.

13. Ellipsometry

The ellipsometry measurements were carried out in air, on a V-Vase Rotating Analyzer equipped with a HS-190 monochromator ellipsometer from J. A. Woollam Co., Inc, at an incident angle of 65°, 70° and 75° with respect to the surface normal. A two-layer model consisting of a bottom Au layer, for which optical constants were calculated from freshly prepared template-stripped Au surfaces, and a Cauchy layer was used for the fit of the measurement on the SAMs. A chosen value of $A_n = 1.45$, $B_n = C_n = 0$ and $k = 0.01$ at all wavelengths was used to fit the thickness. For every SAM, we measured six different spots in total (either two spots per sample for three samples or three spots per sample for two samples were measured) and report the thicknesses as the average with the standard deviation as the error bars.